

Design of a flexible but robust setup for temperature-dependent electrochemistry down to cryogenic temperatures

Michael F. Fink¹  | Sophie Schönfeld^{1,2} | Constantin Schreck¹ | Gerald Hörner¹ | Birgit Weber¹ 

¹Department of Chemistry, Inorganic Chemistry IV, University of Bayreuth, Bayreuth, Germany

²Present address: Fraunhofer Institute for Environmental, Safety, and Energy Technology UMSICHT, Institute Branch Sulzbach-Rosenberg, Department Renewable Energy, Sulzbach-Rosenberg, Germany

Correspondence

Michael F. Fink and Birgit Weber, Department of Chemistry, Inorganic Chemistry IV, University of Bayreuth, Universitätsstrasse 30, 95447 Bayreuth, Germany.

Email: michael.fink@uni-bayreuth.de and weber@uni-bayreuth.de

Funding information

VolkswagenStiftung

Abstract

Electrochemistry and its analytics are essential in a variety of scientific and technological fields where properties related to reduction-oxidation reactions, so-called redox properties, are to be explored. While methodological standards for experiments are well established at room temperature, this is still untrue at sub-zero/cryogenic temperatures, the conditions required for the survey of (ultra-)rapid processes and their intermediates. Problems due to “hand-waving” temperature regulation/conditioning and common usage of pseudo-reference electrodes renders cryo-electrochemistry a great challenge. Herein, we describe a robust setup for performing reliable cryo-electrochemical experiments down to -80°C . It combines highly stable but flexible temperature conditioning with gas-tight sealing of the electrochemical cell setup. Modification of a commercial palladium hydride reference electrode (PdH RE) allows for rapid temperature cycling under cryogenic conditions in aprotic organic solvents. Validation of the setup with the well-known Ferrocene|Ferrocenium ($\text{Fc}|\text{Fc}^+$) redox couple gave good compliance with literature data at room temperature in a range of organic solvent-based electrolytes. Evaluation of temperature-dependent diffusion kinetic parameters, such as diffusion coefficients (D) and diffusional activation energies ($E_{a,D}$) from CVs at multiple potential scan-rates and temperature levels emphasize the reliability of the presented cryo-electrochemical setup.

KEYWORDS

cryo-electrochemistry, diffusion coefficient, diffusional activation energy, Ferrocene

1 | INTRODUCTION

Electrochemistry and its analytics have soared as the foundation for the identification and exploration of properties related to reduction-oxidation reactions ($\text{Red}=\text{Ox}$

$+ne^-$) [1]. So-called redox properties are of fundamental importance for a manifold of research areas in natural and applied (engineering) sciences [2]. They allow the subtle interpretation of energy flows along potential gradients in complex biological systems, such as the

This is an open access article under the terms of the Creative Commons Attribution License, which permits use, distribution and reproduction in any medium, provided the original work is properly cited.

© 2023 The Authors. *Electroanalysis* published by Wiley-VCH GmbH.

transport of energy and charge in Photosystem II prior to O₂ liberation [3]. On the other hand, redox properties and derived electrochemical figures of merit exert a steering role in current developments towards (more) sustainable energy economy. This includes material search and development for emerging electrochemical energy conversion and storage technologies (e.g., batteries, fuel cells, electrolyzers) [4]. The large majority of these data is accessed by voltammetric techniques, using three-electrode setups immersed in an ion conductive electrolyte at ambient conditions [5]. While this provides a wealth of valuable information, (ultra-)rapid processes and their intermediates can hardly be deciphered (at least) on the time-scale of conventional experiments. To this end, decreasing the temperature, *i. e.*, to sub-zero, or even cryogenic conditions, has previously demonstrated to aid in a sufficient stabilization of transient species and hence allow the kinetics of individual (electro-)chemical steps to become accessible within a measurement attempt [6–14].

To the day, a common strategy to achieve low-temperature/cryogenic conditions remains to immerse conventional test cells in slush/cooling baths consisting of dry ice mixed with organic solvents [15–17], allowing for temperatures as low as -78°C [12, 13, 18]. Drawbacks of such immersion techniques are evident: An accurate temperature conditioning/regulation of the electrolyte solution inside the test cell is missing, particularly problematic during long-term measurement sessions [13, 17]. As temperatures cannot be changed intentionally, a variation requires discontinuous manipulations of the bath [19, 20]. More sophisticated setups, covering these technical issues in terms of cooling jackets, date back to the 1970s [8–10], but hardly made their way as a routine tool. A number of additional problems, increasingly virulent at sub-zero temperatures, refer to the elevated Ohmic potential (*iR*) drop and the contamination of electrolytes with atmospheric oxygen and moisture [8]. More critically, pseudo-reference electrodes are often relied upon for electrochemical measurements below zero degrees. Indeed, simple metal wires (e.g., Pt, Ag), most frequently used as pseudo-reference electrodes, flaw thermodynamic equilibrium and are not ideally nonpolarizable. In addition to that, they are limited with respect to operation conditions, *inter alia*, including temperature variations. All of the above can provoke incomprehensible behavior, to the point of significant potential shift during a measurement [21–25]. As a matter of fact, the implementation of electrochemical measurements at sub-zero, or cryogenic temperature conditions, *i. e.*, cryo-electrochemistry, renders itself an ambitious task.

Herein, we report the design and validation of a variable-temperature electrochemical setup which addresses

the whole of the problems discussed. The electrochemical glass-cell setup provides gas-tight integration for the three-electrode configuration with an optimized *iR* drop, the thermometer for thermostatic feedback, the gas in-/outlet providing solvent-saturated and thermostated Ar, and a modified palladium hydride reference electrode (PdH RE). Straightforward implementation and precise temperature regulation/conditioning allow for reliable and reproducible electrochemical measurements to be carried out at temperatures down to -80°C . Validation of the new cryo-electrochemical setup was based on measuring the Ferrocene|Ferrocenium (Fc|Fc⁺) redox reaction in a number of representative organic solvent-based electrolytes. Diffusion coefficients based on cyclic voltammetry (CV) at multiple potential scan-rates recorded at room temperature were in good agreement with literature data. Going beyond literature precedents, CVs at various temperature levels thus allowed to expand the database to include wider temperature ranges as well as to determine diffusional activation energies towards the oxidation of Fc in the various organic solvents.

2 | DESIGN AND CONSTRUCTION OF THE CRYO-ELECTROCHEMICAL SETUP

2.1 | Electrochemical glass-cell setup and three-electrode configuration

A TC5-type electrochemical glass-cell (BVT Technologies a.s., Strážek, CZ) was used for all cryo-electrochemical measurements. It consists of an inner/main cell chamber with a total electrolyte volume of ~ 15 ml, an outer jacket for temperature conditioning and adapters for the three electrode setup, temperature control and gas in-/outlet (refer to SI section S2 for details on various design-technical aspects and customary/commercially available components used). As a working electrode (WE) and counter electrode (CE) we used a PEEK-embedded 2 mm diameter platinum (Pt) plate electrode (CH Instruments, Inc., Austin, TX, USA) and a Pt wire (BVT Technologies a.s., Strážek, CZ), respectively. The three-electrode setup is completed by the reference electrode (RE), which was mounted in a custom-made Luggin-probe; to this end a modified Mini Hydroflex[®] hydrogen electrode was used (Gaskatel Gesellschaft für Gassysteme durch Katalyse und Elektrochemie mbH, Kassel, DE; detailed description of modifications and the RE compartment, *vide infra*). As can be seen from Figure 1, the given design positions the RE close to the WE, while not substantially shading the active surface or disturbing the field of current lines formed between the WE and CE (details in SI

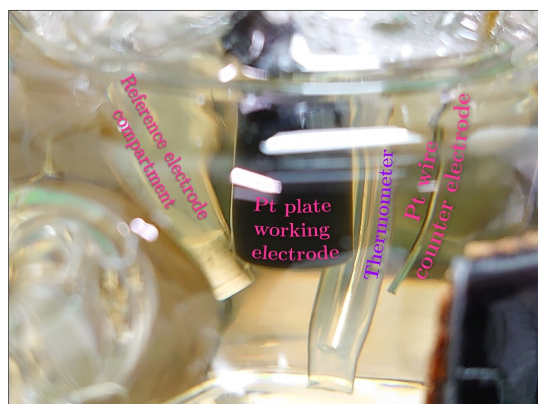


FIGURE 1 View of the three-electrode configuration inside the electrochemical glass-cell setup.

section S2.1). Thereby we minimize the main source of Ohmic potential (iR) drop (see SI section S6.1 for a detailed consideration) [5, 26–29]. More importantly, minimizing the solution resistance is of particular importance as it can increase by multiple with decreasing temperature (see Figure S4).

2.2 | Reference electrode compartment

The RE compartment consists of the Luggin-probe and houses the Mini Hydroflex[®] RE. Moreover, it features a porous glass frit junction at the bottom end. Taking advantage of previous knowledge on the potential variation resulting from electrostatic screening of ion transfer through the frit due to negatively charged surfaces (charge screening), notorious for meso-/nano-porous glass frits [30–34], we have resorted to electro-porous KT glass frits (Koslow Scientific Company, Englewood, NJ, USA) with an average pore diameter of 0.5–1 μm (refer to SI section S2.2 for details on the Luggin-probe) [34]. Similar to previous reports by Mousavi *et al.* [34], a minimal solution flow through the frit within several hours was deemed acceptable (see Figure S2), as herein both the bridge- and test-electrolyte share the same supporting electrolyte.

A Mini HydroFlex[®] RE, which was modified with respect to the hydrogen (H_2) supply, was used as RE in all electrochemical measurements. While conventional hydrogen reference electrodes require prior/constant saturation of the (bridge-)electrolyte solution by H_2 , with Gaskatel's Mini HydroFlex[®] H_2 is provided internally, *i.e.*, *via* a cartridge, that is inserted into the electrode head, and supplied to a gas diffusion electrode (GDE) at the bottom end of the electrode shaft. The GDE consists of a (platinized) Pt mesh incorporated with palladium

(Pd) and PTFE, which is immersed in the electrolyte solution [35]. While this satisfies the principles of a (reversible) hydrogen reference electrode (RHE) in aqueous electrolyte solutions, that is the hydrogen redox reaction ($\text{H}^+_{(\text{aq})} + 1\text{e}^- \rightleftharpoons 0.5\text{H}_{2(\text{g})}$) on Pt eventually establishing the equilibrium potential (*i.e.*, 0.000 V vs. RHE) for measurements at given pH [36–38], this is not valid in aprotic organic solvents [39]. As described above, the Mini HydroFlex[®] RE is also comprised of Pd [35], which exhibits a strong solubility towards H_2 , that is up to ~ 1000 times its volume of dissolved hydrogen within the crystal structure [39–42]. Such formed palladium hydride (PdH) is capable of providing hydrogen cations and thus establishing a reversible hydrogen electrode even in aprotic organic solvents has been demonstrated by Patrick *et al.* [39]. and Gaskatel [44], respectively.

Besides the advantages of the Mini HydroFlex[®] RE, the reliance on H_2 supplied from cartridges carries few operational burdens. *Inter alia*, due to the modest H_2 generation rate from the cartridge fluctuations in pressure owing to the volumetric change of H_2 inside the electrode in wide temperature ranges may cause serious damage to the electrode. This requirement of operation at lowest temperatures and under rapid temperature changes was met through the development of a particular RE setup. As shown by the process flow chart in Figure 2, H_2 was supplied externally *via* a gas cylinder at a constant flow rate and overpressure, that not only balances the volumetric change of H_2 due to the large temperature gradients, but also ensures the preservation of an equilibrium potential with H_2 as well as a pristine PdH layer (refer to SI section S2.2 for more details on the RE setup).

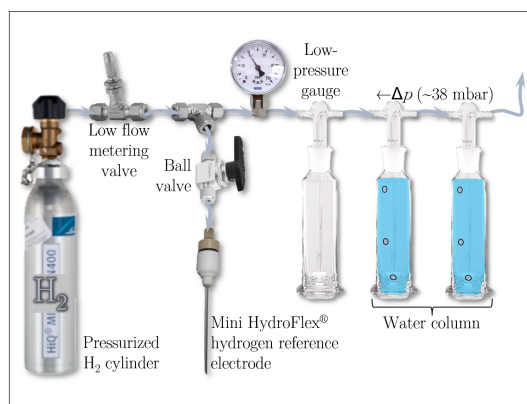


FIGURE 2 Process flow chart of the RE setup for supplying the Mini Hydroflex[®] RE with H_2 at a constant overpressure (38 mbar) and flow rate (~ 1 bubble per second).

2.3 | Gas in-/outlet

Flushing of the glass-cell with inert gas (e.g., for sample filling or saturation with Ar) proceeds *via* an additional gas in-/outlet (refer to SI section S2.3 for a detailed description). Moreover, in order to reduce the loss of electrolyte, Ar was saturated with the thermostated solvent before entering the glass-cell (see Figure 3).

2.4 | Temperature regulation

Variable temperature conditions were accomplished by means of an external thermostatic circulator, model PRO RP 290 E (LAUDA Dr. R. Wobser GmbH & Co. KG, Lauda-Königshofen, DE) with an operational temperature range of $-90 < \vartheta < +200$ °C and a temperature stability of ± 0.05 °C, which was connected to the jacket of the electrochemical glass-cell. Temperature is directly regulated to the main cell chamber using an external thermometer, which is immersed in the electrolyte solution (refer to SI section S2.4 for details). After reaching a certain temperature level, temperature conditioning was maintained for at least 15 min to achieve as constant a temperature of the electrolyte solution (including Luggin-probe) as possible. In this study the temperature was varied between -80 °C (ethanol) and $+80$ °C (tap water) by 10 °C intervals and 1 °C min^{-1} ramps.

2.5 | Electrochemical analyzer

A computer-controlled electrochemical analyzer, model CHI610E (CH Instruments, Inc., Austin, TX, USA) was used for all (cryo-)electrochemical measurements. All data was corrected for the Ohmic potential (iR) drop by means of the instrument's built-in iR compensation

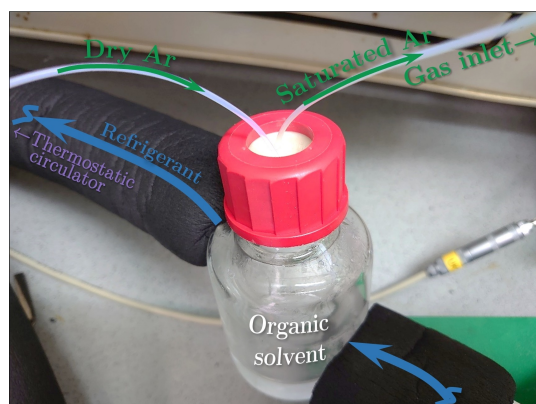


FIGURE 3 Temperature conditioning and solvent saturation of Ar before the gas inlet to the electrochemical glass-cell setup.

technique based on “positive feedback” [45,46], which was performed prior to every measurement. To avoid potential oscillations, we applied a partial 80% compensation to account for the vast iR drop [28,47–49]. Data was acquired with the latest CHI software v18.05 (CH Instruments, Inc., Austin, TX, USA).

3 | VALIDATION AND DISCUSSION OF RESULTS

3.1 | Room temperature measurements

The assembled cryo-electrochemical cell setup with all external connections is illustrated in Figure 4 (please find detailed descriptions on preparatory procedures and the assembly in SI section S3 [50,51]). It was field-tested with the Ferrocene|Ferrocenium ($\text{Fc}|\text{Fc}^+$) redox couple (eqn. S1, structural formulae in Figure 5 top-left).

CVs recorded of $\text{Fc}|\text{Fc}^+$ in a representative selection of organic solvent-based electrolytes including DCM, THF, DMF, DMSO and pyridine (0.1 M NBu_4PF_6 ; 0.001 M $[\text{Fe}(\text{C}_5\text{H}_5)_2]$; $\nu = 0.1$ Vs^{-1}) at 20 °C are presented in Figure 5. Generally, smooth CVs exhibiting the typical “duck” shaped response of the $\text{Fc}|\text{Fc}^+$ redox couple prevail in all electrolytes. It also holds for all potential scan-rates investigated herein (*cf.* DCM at 20 °C in Figure S5 by way of example) [52]. It has been reported previously that the redox potentials of $\text{Fc}|\text{Fc}^+$ are dependent on the solvent reorganization energy [53]. In this respect, Noviantri *et al.* recorded half-wave potentials ($E_{1/2}$; see eqn. S2) between $+0.157$ V $< E_{1/2} < +0.629$ V across a broad range of solvents. When focusing on the five solvents used also in our study, the range narrows to $+0.505$ V (DMSO) $< E_{1/2} < +0.629$ V (THF) [54]. Tsierekos reported in a related but less exhaustive study a range of ca. 200 mV when going from DMSO ($E_{1/2} =$

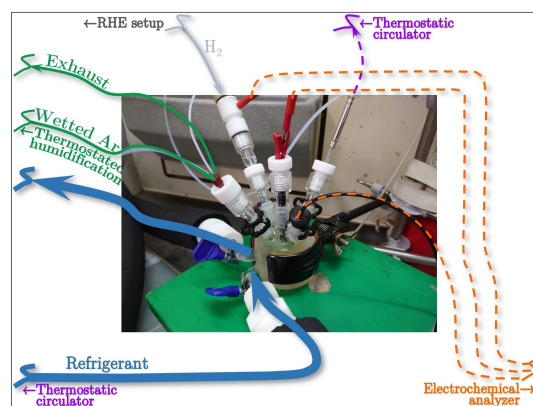


FIGURE 4 Completely assembled cryo-electrochemical glass-cell setup showing all external connections.

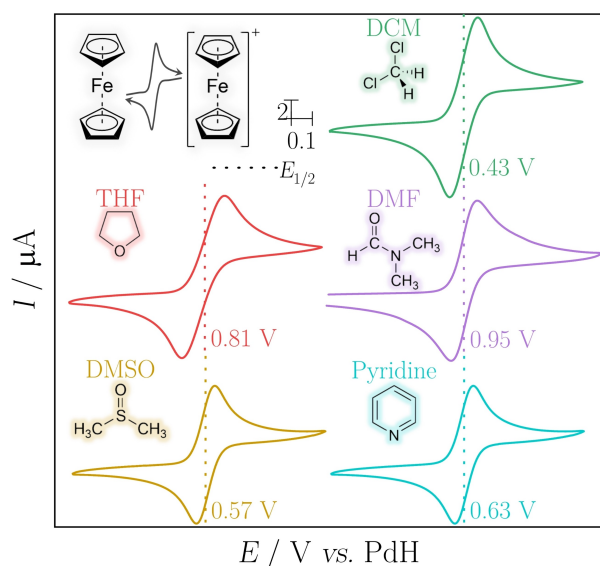


FIGURE 5 Exemplary CVs of $\text{Fc}|\text{Fc}^+$ on a 2 mm diameter Pt plate WE in DCM, THF, DMF, DMSO and Pyridine (0.1 M NuBu_4PF_6 ; 0.001 M $[\text{Fe}(\text{C}_5\text{H}_5)_2]$) at 20 °C, $\nu=0.1 \text{ V s}^{-1}$, including half-wave potentials ($E_{1/2}$). Each CV represents the last of three consecutive measurements. Top-left: Structural formulae of the $\text{Fc}|\text{Fc}^+$ redox reaction.

0.868 V) to DCM ($E_{1/2}=1.094 \text{ V}$) [55]. Similarly, we also find a significant solvent dependence of the $\text{Fc}|\text{Fc}^+$ redox reaction, or $E_{1/2}$, respectively, ranging from +0.43 V (DCM) up to +0.95 V (DMF).

Peak currents were extracted from CVs at multiple potential scan-rates. With increasing potential scan-rate both the peak currents and the separation of the anodic and cathodic peaks increase in a characteristic manner. The typical “trumpet” plots featuring the peak-to-peak separation as a function of logarithmic potential scan-rates are exemplified in Figure S6 by data derived at 20 °C [52, 56]. While this is a characteristic of the $\text{Fc}|\text{Fc}^+$ redox couple to undergo reversible electron-transfer processes [57–59], variations in its form can be attributed to the organic solvents exhibiting different solution resistance [60–64], and hence R_u , as has been previously discussed (SI section S6.1).

For an analysis of diffusion-kinetic data, the peak currents were treated in terms of the Randles-Ševčík equation which allows access to diffusion coefficients (*cf.* eqn. S3) [65–67]. As exemplified by data derived at 20 °C in Figure S7, the linear Randles-Ševčík plots (I_p vs. $\nu^{0.5}$) indicate the electrode process to be largely diffusion-controlled (for the temperature dependence, *vide infra*) [52]. Diffusion coefficients were extracted from the slopes of best fits according to eqn. S4 and eqn. S5. Eventually, Table 1 summarizes such-way determined diffusion coefficients for the oxidation of Fc in the various organic solvent-based electrolytes at 25 °C. Comparison to

reference values reveals good agreement with literature data (see SI section S6.6 for a more detailed consideration). To the best of our knowledge, for pyridine no D values are reported to date. With a view to the omnipresence of pyridine as a medium in coordination chemistry as a whole, not at least in our previous work [68–70], we aimed to close this gap.

The diffusion coefficient of Fc in pyridine is found to be close to that in DMF. This coincidence can be attributed to similar viscosities of both solvents (see Table S1 for details) [71]. Additionally, it is also supported by the linear Stokes-Einstein plot in Figure S8, whose required inverse proportionality between the diffusion coefficient of the species and the viscosity of the organic solvent (*cf.* eqn. S6) holds across the entire set of media [72, 73].

3.2 | Measurements at variable temperature

We opted for temperature ranges $\sim 10^\circ\text{C}$ above the melting and below the boiling point of the solvent, or -80°C to $+80^\circ\text{C}$, respectively. Accordingly, a library of CVs at various potential scan-rates and temperature levels incremented by 10°C steps were recorded in the five aprotic solvents. This is exemplified in Figure 6 by means of the DCM-based electrolyte, which was measured at $-80^\circ\text{C} < \vartheta < +30^\circ\text{C}$ (refer to SI section S6.8 for other solvents). Clearly, while the electrochemical signature of $\text{Fc}|\text{Fc}^+$ is indifferent to temperature, as the temperature decreases, CVs steadily decline accompanied by increasing peak-to-peak separation. This can be ascribed to mass- and electron-transfer becoming more and more sluggish as the temperature drops [13, 14]. The pronounced shifts of CVs in DMSO are conspicuous. However, as DMSO has strong coordination ability, we attribute this to a solvent coordination effect with Pt and Pd, *i.e.*, the electrode materials, that interferes with the

TABLE 1 Diffusion coefficients (D) for the oxidation of Ferrocene on a 2 mm diameter Pt plate WE in DCM, THF, DMF, DMSO and Pyridine (0.1 M NuBu_4PF_6 ; 0.001 M $[\text{Fe}(\text{C}_5\text{H}_5)_2]$) at 25 °C in comparison to literature data at around room temperature.

Solvent	D ($10^{-5} \text{ cm}^2 \text{ s}^{-1}$)	
	This study[a]	Literature
DCM	1.45	1.4 [74]
THF	1.39	1.50 [71]
DMF	1.02	0.95–1.1 [55, 71, 75–78]
DMSO	0.71	0.44–0.67 [55, 71, 79, 80]
Pyridine	0.92	–

[a] interpolated based on D values at 20 °C and 30 °C.

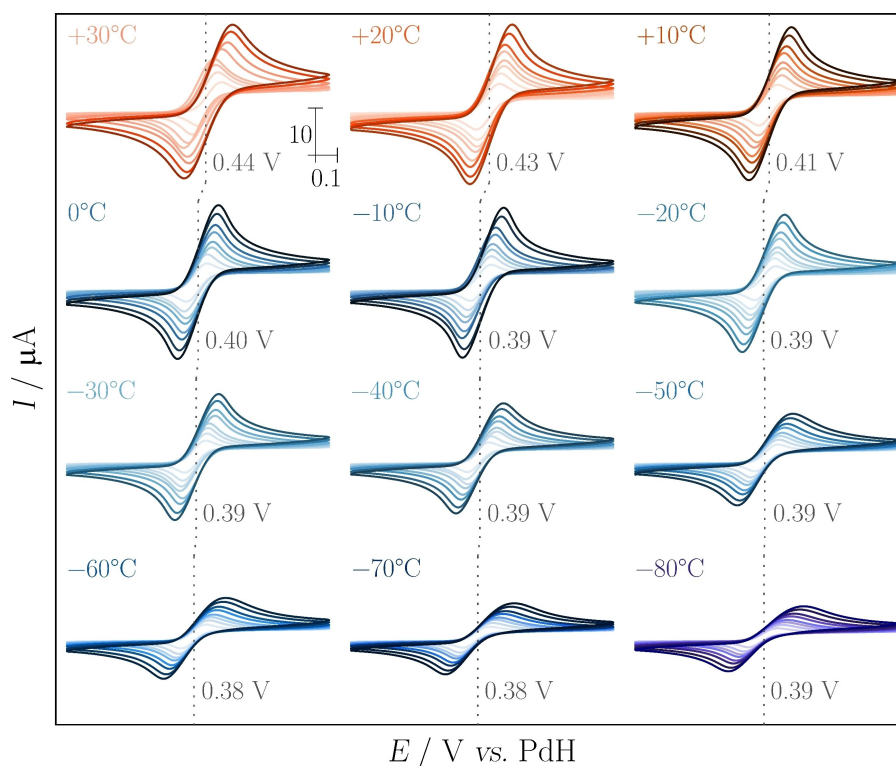


FIGURE 6 CVs of $\text{Fc}|\text{Fc}^+$ at multiple potential scan-rates (0.025, 0.05, 0.075, 0.1, 0.15, 0.2, 0.3, and 0.4 V s^{-1}) on a 2 mm diameter Pt plate WE in DCM (0.1 M NuBu_4PF_6 ; 0.001 M $[\text{Fe}(\text{C}_5\text{H}_5)_2]$) between -80°C and $+30^\circ\text{C}$ at various temperature levels incremented by 10°C steps. Each set of CVs represents the last of three consecutive measurements. Intensifying colors within a set of CVs indicate the increase of potential scan-rate. Minor shifts of CVs at 30°C along the abscissa are due to a change in solution resistance during the measurement.

measurement (refer to DMSO in SI section S6.8 for a detailed consideration) [81,82].

An intriguing feature emerges for the data derived in DCM-based electrolyte, but similarly shines up also in the other solvents: Half-wave potentials shift slightly anodically when the temperature is increased. However, this conflicts with the Nernst equation (see eqn. S7), which essentially demands the opposite [39]. Interestingly, we are not the first to discover “anti-Nernst” behavior, as similar observations have recently been reported by Patrick *et al.* for a PdH RE in aprotic solvent-based electrolytes upon increasing the hydrogen pressure, *i.e.*, from ~ 0.04 to ~ 1.01 bar. As a matter of fact, temperature can cause a comparable change in pressure as well, insofar the solvent’s vapor pressure gives a significant contribution to the overall pressure [38]. For instance, while the vapor pressure of DCM at -80°C is negligible (0.30×10^{-3} bar), it increases to as high as 0.73 bar at $+30^\circ\text{C}$ (other solvents were measured at a significantly larger temperature difference) [83]. We can therefore draw similar conclusions to Patrick *et al.* as regards the positive voltage shift of the Mini HydroFlex® PdH RE. In addition to that, we believe that thermodiffusion/thermophoresis, *i.e.*, the so-called Soret effect, which can arise due to different heat capacities of the

solvents and electrode materials, is implicated (comprehensive discussion in SI section S5) [84–87].

As outlined in the previous section on diffusion coefficients at room temperature, the temperature-dependence of diffusion kinetic parameters was addressed in terms of the Randles-Ševčík equation (Figure 7 considering DCM a case in point, refer to SI section S6.9 for other solvents). The such-derived set of temperature-dependent diffusion coefficients of Fc in various organic solvent-based electrolytes is summarized in Table S3. Due to the previous lack of a flexible setup for electrochemical measurements in broad temperature ranges, reference data were available mostly at and around room temperature. While a comprehensive cross-check is therefore impossible, the extracted diffusion coefficients at room temperature could be convincingly cross-validated with literature data, thus lending reliability to our data.

The validity of our data has been further assessed through the determination of diffusional activation energies *via* the Arrhenius approach [88]. Arrhenius plots of the logarithmic diffusion coefficients as a function of inverse temperature are presented in Figure 8a. Excellent linearity over the investigated temperature range prevails in all cases ($R^2 = 0.98\text{--}1.0$) allowing for the

extraction of diffusional activation energies *via* the “linearized” Arrhenius equation (eqn. S8), or by the slopes of best fits (lin. reg.) to the Arrhenius plots, respectively, according to eqn. S9 [89–91]. Such-derived diffusional activation energies are presented in Figure 8b and follow the order DMF ($24.8 \pm 0.2 \text{ kJ mol}^{-1}$) \gg Pyridine ($14.5 \pm 0.7 \text{ kJ mol}^{-1}$) $>$ DCM ($13.0 \pm 0.7 \text{ kJ mol}^{-1}$) $>$ DMSO ($12.6 \pm 0.1 \text{ kJ mol}^{-1}$) $>$ THF ($9.9 \pm 0.3 \text{ kJ mol}^{-1}$). While this is the most comprehensive study evaluating diffusion kinetic parameters over broad temperature ranges as of yet, a comparison with literature is not

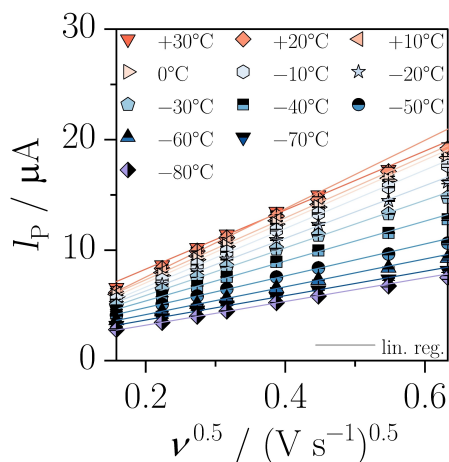


FIGURE 7 Temperature-dependent Randles-Ševčík plots for the oxidation of Fc on a 2 mm diameter Pt plate WE in DCM ($0.1 \text{ M NuBu}_4\text{PF}_6$; $0.001 \text{ M [Fe(C}_5\text{H}_5)_2]$) between -80°C and $+30^\circ\text{C}$ at various temperature levels incremented by 10°C steps. Symbols: Average including standard deviation based on three consecutive measurements ($\sigma = \pm 0.72$). The experimental data has been approximated by best fits (lin. reg., $R^2 = 0.99\text{--}1.0$). Note, a constant symmetry barrier coefficient ($\alpha = 0.5 = \text{const.}$) is assumed [67].

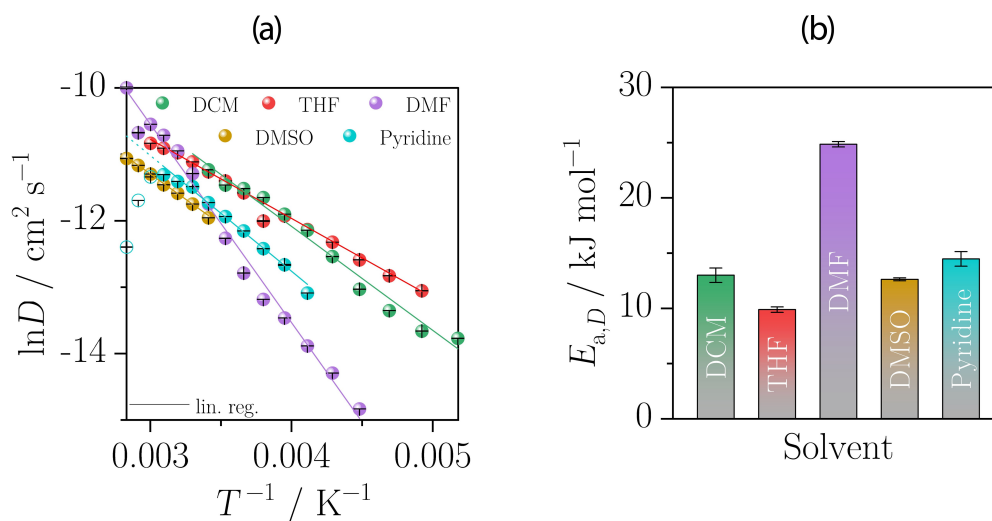


FIGURE 8 (a) Arrhenius plots including best fits (lin. reg., $R^2 = 0.98\text{--}1.0$) and (b) diffusional activation energies ($E_{a,D}$) for the oxidation of Fc on a 2 mm diameter Pt plate WE in DCM, THF, DMF, DMSO and Pyridine ($0.1 \text{ M NuBu}_4\text{PF}_6$; $0.001 \text{ M [Fe(C}_5\text{H}_5)_2]$). Symbols/bars: Average values including standard deviation based on three consecutive measurements.

easily feasible (similar to temperature dependent diffusion coefficients, as discussed above). Although the majority of reported diffusional activation energies for Fc as based on few temperature levels starting from room temperature upwards, the $E_{a,D}$ values presented herein are of a similar order of magnitude (see SI section S6.11 for examples).

We note that the Arrhenius treatment of the data in pyridine had to be limited to $\vartheta < +60^\circ\text{C}$. At elevated temperature we observed a sudden, irreversible drop of the diffusion coefficients that is likewise evident from significantly declining CVs (see Figure S11). For instance, D at $+80^\circ\text{C}$ has declined to $0.41 \times 10^{-5} \text{ cm}^2 \text{ s}^{-1}$, matching the data at $\vartheta = -30^\circ\text{C}$. Consequently, we repeated the series (not shown). The same irreversible decline of CVs and diffusion coefficients is observed $> +60^\circ\text{C}$. Thermally-induced decomposition of Fc or Fc^+ can be discarded, as has been demonstrated by measurements up to $+80^\circ\text{C}$ in other solvents. Rather, all the evidence suggests a thermal reaction of Fc and or Fc^+ with pyridine.

4 | SUMMARY

At present, recording of valid electrochemical information at cryogenic temperature conditions is not a routine task. While *ad-hoc* setups relying on immersion in stationary cooling baths can usually cope with a few of the low-temperature inherent challenges, lacking precise temperature regulation/conditioning and reliable reference potential assessment massively affect reproducibility among the measurements, even within the same

laboratory. Herein we provide a detailed technical report and discussion of the design and construction of a robust temperature-variable electrochemical setup, particularly laid out for electrochemical measurements at cryogenic conditions. Technical approaches to precise temperature conditioning with a stability of ± 0.05 K and the strict exclusion of atmospheric intrusions are given in detail. Gas-tight integration of all components into the electrochemical glass-cell resulted in a highly reproducible arrangement of the three-electrode setup exhibiting a minimal iR drop, the thermometer for temperature control and the gas in-/outlet for providing thermostated and solvent-saturated Ar. The need for flexible variation of temperature likewise required the modification of a commercially available palladium hydride reference electrode (PdH RE). PdH RE is modified by means of H_2 supplied *via* an external RE setup such as to endure operation at cryogenic conditions under rapid temperature cycling in aprotic organic solvents. Operational capability and reliability of the cryo-electrochemical setup was validated by cyclic voltammetry (CV) of the $Fc|Fc^+$ redox couple in a number of representative organic solvent-based electrolytes including DCM, THF, DMF, DMSO and pyridine. From CVs at multiple potential scan-rates and temperature levels we extracted temperature-dependent diffusion coefficients (D) and diffusional activation energies ($E_{a,D}$) towards the oxidation of Fc. While good agreement was found with literature values at room temperature, we were able to expand the database to include wider temperature ranges. Thus, besides providing a comprehensive data set towards temperature-dependent diffusion kinetic parameters in the various organic solvent-based electrolytes, the detailed descriptions given herein, will allow the interested fellow researchers to easily replicate setups and procedures, removing hurdles on performing accurate and reliable temperature-dependent electrochemical measurements in the future.

AUTHOR CONTRIBUTIONS

The manuscript was written through contributions of all authors.

ACKNOWLEDGMENTS

The authors gratefully acknowledge financial support by the VolkswagenStiftung, funding initiative “Experiment!” (Spin Batt). Thanks are due to Dr. H.-J. Kohnke and Mr. J. Helmke from Gaskatel (Gaskatel Gesellschaft für Gassysteme durch Katalyse und Elektrochemie mbH, Kassel, DE) for stimulating discussions towards their Mini HydroFlex[®] reference electrode. Eventually, we highly appreciate Mr. M. Dittrich, Mr. M. Groll and staff

from the university’s in-house glassblowing studio and mechanics workshop for manufacturing numerous custom-made components. Open Access funding enabled and organized by Projekt DEAL.



CONFLICT OF INTEREST STATEMENT

The authors declare no conflict of interest.

DATA AVAILABILITY STATEMENT

The data that support the findings of this study are available from the corresponding author upon reasonable request.

ORCID

Michael F. Fink  <http://orcid.org/0000-0002-2039-4735>
Birgit Weber  <http://orcid.org/0000-0002-9861-9447>

REFERENCES

1. D. A. C. Brownson, C. E. Banks in *The Handbook of Graphene Electrochemistry* (Eds.: D. A. C. Brownson, C. E. Banks), Springer London, London, **2014**, pp. 23–77.
2. J. H. Zagal, I. Ponce, R. Oñate in *Redox* (Eds.: R. Khattak), IntechOpen, **2020**, pp. 1–24.
3. F. Rappaport, B. Diner, *Coord. Chem. Rev.* **2008**, *252*, 259–272.
4. S. P. S. Badwal, S. S. Giddey, C. Munnings, A. I. Bhatt, A. F. Hollenkamp, *Front. Chem.* **2014**, *2*, 1–28.
5. in *Electrochemical Methods: Fundamentals and Applications, 2nd ed.* (Eds.: A. J. Bard, L. R. Faulkner), Wiley, New York, Weinheim, **2001**, pp. 1–43.
6. J. T. McDevitt, S. Ching, M. Sullivan, R. W. Murray, *J. Am. Chem. Soc.* **1989**, *111*, 4528–4529.
7. D. K. Gosser, Q. Huang, *J. Electroanal. Chem. Interfacial Electrochem.* **1989**, *267*, 333–338.
8. R. P. van Duyne, C. N. Reilley, *Anal. Chem.* **1972**, *44*, 142–152.
9. R. P. van Duyne, C. N. Reilley, *Anal. Chem.* **1972**, *44*, 153–158.
10. R. P. van Duyne, C. N. Reilley, *Anal. Chem.* **1972**, *44*, 158–169.
11. C. A. Paddon, F. L. Bhatti, T. J. Donohoe, R. G. Compton, *J. Electroanal. Chem.* **2006**, *589*, 187–194.
12. N. Fietkau, C. A. Paddon, F. L. Bhatti, T. J. Donohoe, R. G. Compton, *J. Electroanal. Chem.* **2006**, *593*, 131–141.
13. I. López, N. Le Poul, *Coord. Chem. Rev.* **2021**, *436*, 213823.
14. I. López, N. Le Poul, *J. Electroanal. Chem.* **2021**, *887*, 115160.
15. R. J. Wilson, L. F. Warren, M. F. Hawthorne, *J. Am. Chem. Soc.* **1969**, *91*, 758–759.
16. L. L. Miller, E. A. Mayeda, *J. Am. Chem. Soc.* **1970**, *92*, 5818–5819.
17. P.-Y. Chien, L. Cheng, C.-Y. Liu, J.-E. Li, B. T.-H. Lee, *Acta Mater.* **2021**, *204*, 116486.
18. T. J. Donohoe, D. J. Johnson, R. G. Compton, J. D. Wadhawan, *Tetrahedron* **2004**, *60*, 5945–5952.
19. R. E. Rondeau, *J. Chem. Eng. Data* **1966**, *11*, 124.
20. A. M. Phipps, D. N. Hume, *J. Chem. Educ.* **1968**, *45*, 664.
21. G. Inzelt in *Handbook of Reference Electrodes* (Eds.: G. Inzelt, A. Lewenstam, F. Scholz), Springer Berlin Heidelberg, Berlin, Heidelberg, **2013**, pp. 331–332.
22. H. Kahlert in *Electroanalytical Methods* (Eds.: F. Scholz, A. M. Bond, R. G. Compton, D. A. Fiedler, G. Inzelt, H. Kahlert, Š.

- Komorsky-Lovrić, H. Lohse, M. Lovrić, F. Marken, A. Neudeck, U. Retter, F. Scholz, Z. Stojek), Springer Berlin Heidelberg, Berlin, Heidelberg, **2010**, pp. 291–308.
23. A. J. Bard, G. Inzelt, F. Scholz in *Electrochemical Dictionary* (Eds.: A. J. Bard, G. Inzelt, F. Scholz), Springer Berlin Heidelberg, Berlin, Heidelberg, **2012**, pp. 781–815.
 24. A. J. Bard, G. Inzelt, F. Scholz in *Electrochemical Dictionary* (Eds.: A. J. Bard, G. Inzelt, F. Scholz), Springer Berlin Heidelberg, Berlin, Heidelberg, **2012**, pp. 773–779.
 25. in *Electrochemical Methods: Fundamentals and Applications, 2nd ed.* (Eds.: A. J. Bard, L. R. Faulkner), Wiley, New York, Weinheim, **2001**, pp. 44–86.
 26. F. Zhang, J. Liu, I. Ivanov, M. C. Hatzell, W. Yang, Y. Ahn, B. E. Logan, *Biotechnol. Bioeng.* **2014**, *111*, 1931–1939.
 27. A. Battistel, M. Fan, J. Stojadinović, F. La Mantia, *Electrochim. Acta* **2014**, *135*, 133–138.
 28. S. Anantharaj, S. Noda, *J. Mater. Chem. A* **2022**, *10*, 9348–9354.
 29. T. Kakiuchi, *J. Solid State Electrochem.* **2011**, *15*, 1661–1671.
 30. E. L. Anderson, S. A. Saba, D. J. Loomis, P. Bühlmann, M. A. Hillmyer, *ACS Appl. Nano Mater.* **2018**, *1*, 139–144.
 31. E. L. Anderson, T. P. Lodge, T. Gopinath, G. Veglia, P. Bühlmann, *Anal. Chem.* **2019**, *91*, 7698–7704.
 32. E. L. Anderson, B. K. Troutdt, P. Bühlmann, *Anal. Sci.* **2020**, *36*, 187–191.
 33. M. P. S. Mousavi, P. Bühlmann, *Anal. Chem.* **2013**, *85*, 8895–8901.
 34. M. P. S. Mousavi, S. A. Saba, E. L. Anderson, M. A. Hillmyer, P. Bühlmann, *Anal. Chem.* **2016**, *88*, 8706–8713.
 35. Gaskatel Gesellschaft für Gassysteme durch Katalyse und Elektrochemie mbH, Kassel, DE. https://gaskatel.de/wp-content/uploads/Manual_Mini_HydroFlex_V2-1.pdf (accessed 23–05–15).
 36. O. Boisen, A. Corral, E. Pope, J. C. Goeltz, *J. Chem. Educ.* **2019**, *96*, 1418–1423.
 37. J. A. Zamora Zeledón, A. Jackson, M. B. Stevens, G. A. Kamat, T. F. Jaramillo, *J. Electrochem. Soc.* **2022**, *169*, 66505.
 38. G. Jerkiewicz, *ACS Catal.* **2020**, *10*, 8409–8417.
 39. B. N. Patrick, R. Chakravarti, T. M. Devine, *J. Electrochem. Soc.* **2016**, *163*, H171–H179.
 40. P. Leuaa, C. Chatzichristodoulou, *J. Electrochem. Soc.* **2022**, *169*, 54534.
 41. S. Dekura, H. Kobayashi, K. Kusada, H. Kitagawa, *ChemPhys-Chem* **2019**, *20*, 1158–1176.
 42. M. J. Vasile, C. G. Enke, *J. Electrochem. Soc.* **1965**, *112*, 865–870.
 43. in *Interfacial Electrochemistry: An Experimental Approach* (Eds.: E. Gileadi, E. Kirowa-Eisner, J. Penciner, E. Gileadi, J. Penciner), Addison-Wesley, Massachusetts, **1975**, pp. 206–232.
 44. H.-J. Kohnke, Frankfurt am Main, DE, **2009**. https://nanopdf.com/download/wasserstoff-referenz-elektroden-in-organischen_pdf (accessed 23–05–15).
 45. in *Electrochemical Methods: Fundamentals and Applications, 2nd ed.* (Eds.: A. J. Bard, L. R. Faulkner), Wiley, New York, Weinheim, **2001**, pp. 632–658.
 46. CH Instruments, Inc., <https://www.chinstruments.com/chi600.shtml> (accessed 23-05-15).
 47. A. R. Heenan, J. Hamonnet, A. T. Marshall, *ACS Energy Lett.* **2022**, *7*, 2357–2361.
 48. P. He, L. R. Faulkner, *Anal. Chem.* **1986**, *58*, 517–523.
 49. W. Oelßner, F. Berthold, U. Guth, *Mater. Corros.* **2006**, *57*, 455–466.
 50. M. F. Fink, J. Eckhardt, P. Khadke, T. Gerdes, C. Roth, *Chem-ElectroChem* **2020**, *7*, 4822–4836.
 51. M. F. Fink, M. Weiss, R. Marschall, C. Roth, *J. Mater. Chem. A* **2022**, *10*, 15811–15838.
 52. N. Elgrishi, K. J. Rountree, B. D. McCarthy, E. S. Rountree, T. T. Eisenhart, J. L. Dempsey, *J. Chem. Educ.* **2018**, *95*, 197–206.
 53. in *Electrochemical Methods: Fundamentals and Applications, 2nd ed.* (Eds.: A. J. Bard, L. R. Faulkner), Wiley, New York, Weinheim, **2001**, pp. 87–136.
 54. I. Noviandri, K. N. Brown, D. S. Fleming, P. T. Gulyas, P. A. Lay, A. F. Masters, L. Philips, *J. Phys. Chem. B* **1999**, *103*, 6713–6722.
 55. N. G. Tsierkezos, *J. Solution Chem.* **2007**, *36*, 289–302.
 56. E. Laviron, *J. Electroanal. Chem. Interfacial Electrochem.* **101** (1979) 19–28.
 57. F. A. Armstrong, based on the Presentation given at Dalton Discussion No. 4, 10–13th January 2002, Kloster Banz, DE, *J. Chem. Soc., Dalton Trans.* **2002**, 661–671.
 58. J. M. Hudson, K. Heffron, V. Kotlyar, Y. Sher, E. Maklashina, G. Cecchini, F. A. Armstrong, *J. Am. Chem. Soc.* **2005**, *127*, 6977–6989.
 59. M. G. Friedrich, J. W. F. Robertson, D. Walz, W. Knoll, R. L. C. Naumann, *Biophys. J.* **2008**, *94*, 3698–3705.
 60. C. Zhao, G. Burrell, A. A. J. Torriero, F. Separovic, N. F. Dunlop, D. R. MacFarlane, A. M. Bond, *J. Phys. Chem. B* **2008**, *112*, 6923–6936.
 61. S. K. Sukardi, J. Zhang, I. Burgar, M. D. Horne, A. F. Hollenkamp, D. R. MacFarlane, A. M. Bond, *Electrochem. Commun.* **2008**, *10*, 250–254.
 62. J. Zhang, A. M. Bond, *Anal. Chem.* **2003**, *75*, 2694–2702.
 63. J. E. F. Weaver, D. Breadner, F. Deng, B. Ramjee, P. J. Ragonna, R. W. Murray, *J. Phys. Chem. C* **2011**, *115*, 19379–19385.
 64. L. Bahadori, M. H. Chakrabarti, N. S. A. Manan, M. A. Hashim, F. S. Mjalli, I. M. AlNashef, N. Brandon, *PLoS One* **2015**, *10*, 1–21.
 65. J. E. B. Randles, *Trans. Faraday Soc.* **1948**, *44*, 327–338.
 66. A. Ševčík, *Collect. Czech. Chem. Commun.* **1948**, *13*, 349–377.
 67. in *Electrochemical Methods: Fundamentals and Applications, 2nd ed.* (Eds.: A. J. Bard, L. R. Faulkner), Wiley, New York, Weinheim, **2001**, pp. 226–260.
 68. B. Weber, F. A. Walker, *Inorg. Chem.* **2007**, *46*, 6794–6803.
 69. S. Schlamp, K. Dankhoff, B. Weber, *New J. Chem.* **2014**, *38*, 1965–1972.
 70. C. Lochenie, K. G. Wagner, M. Karg, B. Weber, *J. Mater. Chem. C* **2015**, *3*, 7925–7935.
 71. P. Cassoux, R. Dartiguepeyron, P.-L. Fabre, D. de Montauzon, *Electrochim. Acta* **1985**, *30*, 1485–1490.
 72. A. Einstein, *Ann. Phys.* **1906**, *324*, 289–306.
 73. in *Understanding Voltammetry* (Eds.: R. G. Compton, C. E. Banks), WORLD SCIENTIFIC, **2007**, pp. 153–192.
 74. K. M. Kadish, J. Q. Ding, T. Malinski, *Anal. Chem.* **1984**, *56*, 1741–1744.
 75. M. E. Clark, J. L. Ingram, E. E. Blakely, W. J. Bowyer, *J. Electroanal. Chem.* **1995**, *385*, 157–162.
 76. S. Chanfreau, P. Cognet, S. Camy, J.-S. Condoret, *J. Electroanal. Chem.* **2007**, *604*, 33–40.

77. S. R. Jacob, Q. Hong, B. A. Coles, R. G. Compton, *J. Phys. Chem. B* **1999**, *103*, 2963–2969.
78. A. J. Zara, S. S. Machado, L. O. S. Bulhões, A. V. Benedetti, *J. Electroanal. Chem. Interfacial Electrochem.* **1987**, *221*, 165–174.
79. A. Salmon, Dissertation, Bielefeld University, 2001.
80. J. Janisch, A. Ruff, B. Speiser, C. Wolff, J. Zigelli, S. Benthin, V. Feldmann, H. A. Mayer, *J. Solid State Electrochem.* **2011**, *15*, 2083–2094.
81. M. D. Hall, K. A. Telma, K.-E. Chang, T. D. Lee, J. P. Madigan, J. R. Lloyd, I. S. Goldlust, J. D. Hoeschele, M. M. Gottesman, *Cancer Res.* **2014**, *74*, 3913–3922.
82. T. Diao, P. White, I. Guzei, S. S. Stahl, *Inorg. Chem.* **2012**, *51*, 11898–11909.
83. J. H. Perry, *J. Phys. Chem.* **1927**, *31*, 1737–1741.
84. H. J. V. Tyrrell, R. Colledge, *Nature* **1954**, *173*, 264–265.
85. E. D. Eastman, *J. Am. Chem. Soc.* **1928**, *50*, 283–291.
86. J. J. Mentor, R. Torres, D. T. Hallinan, *Mol. Syst. Des. Eng.* **2020**, *5*, 856–863.
87. W. Köhler, K. I. Morozov, *J. Non-Equilib. Thermodyn.* **2016**, *41*, 151–197.
88. S. Arrhenius, *Z. Phys. Chem.* **1889**, *4 U*, 96–116.
89. Y. Wang, E. I. Rogers, R. G. Compton, *J. Electroanal. Chem.* **2010**, *648*, 15–19.
90. M. Matsumiya, M. Terazono, K. Tokuraku, *Electrochim. Acta* **2006**, *51*, 1178–1183.
91. E. I. Rogers, D. S. Silvester, D. L. Poole, L. Aldous, C. Hardacre, R. G. Compton, *J. Phys. Chem. C* **2008**, *112*, 2729–2735.

SUPPORTING INFORMATION

Additional supporting information can be found online in the Supporting Information section at the end of this article.

How to cite this article: M. F. Fink, S. Schönfeld, C. Schreck, G. Hörner, B. Weber, *Electroanalysis* **2023**, *35*, e202300154.
<https://doi.org/10.1002/elan.202300154>